3rd European supercritical CO2 Conference
September 19-20, 2019, Paris, France

2019-sCO2.eu-111

INVESTIGATION OF A CORRELATION BASED MODEL FOR SCO2 COMPACT HEAT EXCHANGERS

Markus Hofer*
University of Stuttgart
Stuttgart, Germany
markus.hofer@ike.uni-stuttgart.de

Michael Buck
University of Stuttgart
Stuttgart, Germany

Marcel Strätz
University of Stuttgart
Stuttgart, Germany

Jörg Starflinger
University of Stuttgart
Stuttgart, Germany

ABSTRACT

Motivated by the Fukushima accident, innovative heat removal systems for nuclear power plants are currently under investigation. One of them is the supercritical carbon dioxide (sCO_2) heat removal system, a closed Brayton cycle with sCO_2 as working fluid. ATHLET (Analysis of THermal-hydraulics of LEaks and Transients) has been used to simulate the interaction of the heat removal system with the nuclear power plant. However, the component models need further development and validation.

In this paper, a general approach for the simulation of heat exchangers is applied to a compact heat exchanger (CHX), including the heat transfer and pressure drop correlations used in ATHLET. Based on stationary experiments of a two-plate CHX, dimensionless form loss coefficients for the sCO_2 inlet and outlet plenum are derived. In a second step, these coefficients are used as input values for a model, which solves the conservation equations for momentum and energy for a representative H_2O/sCO_2 channel pair. The results of the ATHLET simulations are in good agreement with the experiments. Compared to the mean values of the experiments, almost all simulated cases yield a deviation of less than 10 %, concerning transferred power and the pressure drop on the sCO_2-side.

INTRODUCTION

In case of a station blackout and loss of ultimate heat sink accident scenario in a boiling water reactor (BWR) or pressurized water reactor, the plant accident management strongly depends on the availability of electricity, e.g. provided by emergency diesel generators or external measures. If not available, core integrity will be violated, like in Fukushima Dachii. Such scenarios lead to the development of advanced decay heat removal systems. Since space is a limitation in existing power plants, the supercritical carbon-dioxide (sCO_2) heat removal system "sCO2-HeRo" was proposed [1], [2]. This system consists of a compact heat exchanger, a gas cooler, serving as the ultimate heat sink, and the turbomachinery, one compressor and a turbine mounted on one shaft. Since the turbine is generating more electricity than is used by the compressor and the electrical driven fans of the gas cooler, the system is self-propelling and self-sustaining. The excess electricity can even be used to support other accident measures. sCO_2 is selected as working fluid because of its favorable fluid properties, enabling the design of a very compact system. Moreover, sCO_2 is not combustible, non-toxic and commercially available. The design of a compact system is beneficial because it enables the reduction of material consumption and cost. In the case of the safety system, especially a compact CHX is necessary because the space in the containment of existing reactors is limited. Furthermore, for next generation power cycles reduced material consumption enables steeper transients during the operation.

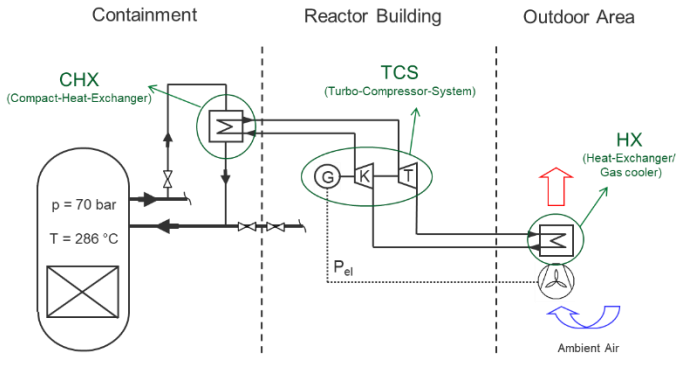

Figure 1: sCO2 heat removal system attached to a BWR [1]

Figure 1 shows a scheme of the sCO2-HeRo system attached to a BWR. In the case of an accident the valves, which connect

DOI: 10.17185/duepublico/48874

the CHX to the main steam line, open automatically. Driven by natural convection, the steam condenses in the primary side of the CHX and thereby heats the sCO_2 in the secondary side of the CHX. The pressurized and heated sCO_2 is expanded in the turbine, which drives the compressor and generates power for the fans of the gas cooler. After the turbine, the remaining heat of the sCO_2 is removed in the gas cooler to the ultimate heat sink. Finally, the sCO_2 is compressed and re-enters the CHX.

For the simulation of the thermo-hydraulic behavior of nuclear power plants, different system codes are used, e.g. CATHARE, RELAP, TRACE and ATHLET [3]. Because sCO_2 is considered as a working fluid for 4th generation reactor concepts as well as for the proposed heat removal system, work is in progress to extend these system codes for the simulation of sCO_2 power cycles [1], [4]–[6]. Venker investigated the feasibility of the sCO2-HeRo approach in detail and implemented first extensions in the ATHLET code for the simulation of the heat removal system. Among other things, heat transfer and pressure drop correlations for sCO_2 were implemented and validated with experimental data. In the frame of the sCO2-HeRo-project further reports and studies were published, including experiments with a two plate CHX [2], [7].

In this paper, these experimental results are used to investigate and validate a correlation-based approach to model a CHX. The extensions and first validations of the thermo-hydraulic system code ATHLET (Analysis of THermal-hydraulics of LEaks and Transients) are summarized and discussed. Firstly, the experiments are briefly described and secondly, the modelling approach and the relevant correlations are explained in detail divided into a general, heat transfer and pressure drop section. Thirdly, the results are discussed in the same manner. In the end, the conclusion provides the most important findings and an outlook to future research activities.

EXPERIMENTS

The two-plate CHX test configuration consists of one H_2O and one sCO_2 plate, each with 15 rectangular channels. A detailed description of the set-up and the conducted experiments by using the SCARLETT test facility and a steam cycle at the IKE is given in [7]. The sCO_2 plate is schematically shown in Figure 2. The channel length is 150 mm and the length of each plenum is 13 mm, which results in a total inner length of 176 mm. The rectangular channels have a width of 2 mm and a height of 1 mm, which is also the height of both plenums. The inlet and outlet pipe of each plenum has an inner diameter of 10.2 mm and is attached perpendicular to the plate. For the H_2O side the geometries are the same. The heat transfer experiment with the CHX were performed in counter-current-flow configuration, so the H_2O and sCO_2 inlet are located at the opposite ends of the two-plate heat exchanger.

The experiments were carried out for three different sCO_2 inlet pressures, namely 9.5 MPa, 10 MPa and 11 MPa. For each inlet pressure, 12 measurements were conducted, mainly with a high H_2O mass flow rate and varying sCO_2 mass flow rates. The sCO_2 inlet temperature was between 38.8 °C and 39.6 °C and the H_2O inlet temperature between 284.8 °C and 285.6 °C. It is assumed that the steam enters the CHX saturated, so the pressure is around 7 MPa.

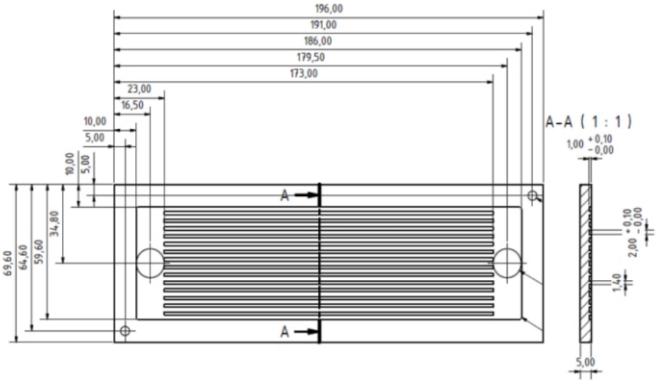

Figure 2: sCO_2 plate [7]

Case 5, which yielded the highest transferred power, is used as a reference in the results section to illustrate the simulation results. The parameters of case 5 are summarized in Table 1.

Table 1: Experimental values of case 5

	Inlet	**Outlet**
p_{SCO2} **in MPa**	10.95	10.91
ϑ_{SCO2} **in °C**	38.8	45.5
$\dot{m}_{SCO2}$ **in g/s**	36.5	
$\dot{Q}_{SCO2}$ **in kW**	1.15	
p_{H2O} **in MPa**	7.03	7.02
ϑ_{H2O} **in °C**	285.5	38.8
$\dot{m}_{H2O}$ **in g/s**	0.50	
$\dot{Q}_{H2O}$ **in kW**	1.30	

Deviations in the calculated transferred powers on the H_2O and sCO_2 side, which can be calculated from the experimental values of both sides, are caused by measurement uncertainties, heat losses and the fact that temperature and pressure are measured not directly at the inlet and outlet of the CHX. This also caused the equality of the sCO_2 inlet and the H_2O outlet temperature. Therefore, the simulated transferred power is compared against the mean of the experimental values.

MODELLING APPROACH

Since the CHX is only one component of the heat removal system and the interaction with the nuclear power plant will be analysed in the future the goal is to develop a fast and sufficiently accurate model. In ATHLET no specific CHX model exists. Therefore, the basic heat exchanger modelling approach was applied. Instead of modelling the entire heat exchanger, only a representative pair of channels is modelled and then scaled by the number of channels. Additionally, the pressure drop in each plenum is modeled by a form loss coefficient. In ATHLET a minimum pressure drop or gain caused by a change in the cross sectional flow area is already considered. However, the measured pressure loss is considerably higher due to the perpendicular attached tubes and the geometry of the plenum.

DOI: 10.17185/duepublico/48874

Therefore, additional form loss coefficients at the inlet and outlet junction of the heat exchanger are necessary. In the experiment, heat transfer also occurs in the plenum. However, due to the geometry of the plenum and the inlet effects, the amount of heat transferred in the plenum is relatively small. Therefore, the plenum is not modelled by an explicit subvolume but is reduced to a junction related pressure drop. Consequently, the length of the CHX in the simulation is equal to the channel length. In Figure 3, the nodalisation of the sCO_2 side is shown.

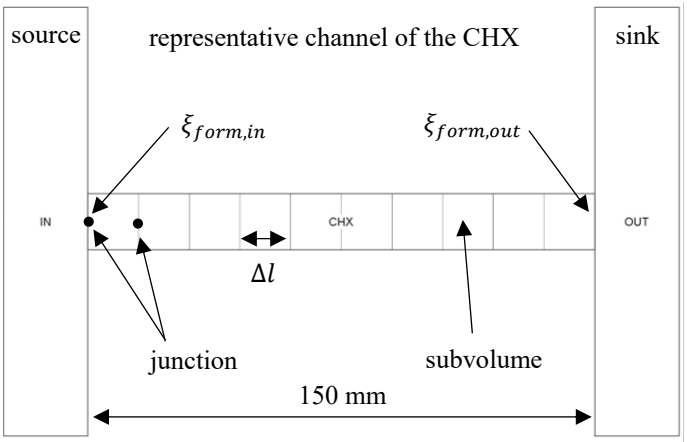

Figure 3: sCO_2 side nodalisation scheme

ATHLET distinguishes between circular channels and other geometries. Other geometries like rectangular channels geometry are characterized by flow area and hydraulic diameter. It is worth noting, that the heat transfer area can be selected independently from the channel geometry if a plate configuration is chosen. The heat transfer area of one subvolume is the product of the channel length and the plate width. The length of one subvolume is fixed by the chosen number of subvolumes but the plate width w and the plate thickness δ can be selected by the user. This plate object, as shown in Figure 4, is the connection between the sCO_2 and H_2O side. In ATHLET it also referred to as heat conduction object.

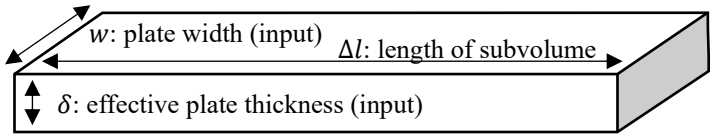

Figure 4: Plate heat conduction in ATHLET (single layer)

For this case, the appropriate plate width and the resulting heat transfer area can be selected by taking into account a few considerations. In the cross-sectional view, the width over which heat is transferred is the perimeter of the channel. However, the temperature distribution and the heat transfer are not uniform, especially for the two-plate configuration. The major part of the heat transfer occurs directly between the two channels, leading to the highest temperature difference in this region. On the opposite side of the plate, which is insulated against heat losses to the environment, the temperature difference and the transferred power are much smaller. In Figure 5, the two-dimensional steady state temperature distribution calculated with a finite volume method inside the two-plate configuration is shown. It is assumed that the heat transfer for each channel is symmetrical. Therefore, the channel middle is located on the right border of the diagram and the middle between to channels on the left border. Since top and bottom are insulated, all boundaries are adiabatic. The symmetry assumption is only partly valid because the total number of channels is small. However, this simulation is sufficient to evaluate the effects of the non-uniform temperature distribution of this configuration. The highest temperature gradient can be observed directly between the channels. However, also the side walls and even the opposite wall contribute to the heat transfer. Therefore, the thermal resistance of the whole configuration should be considered.

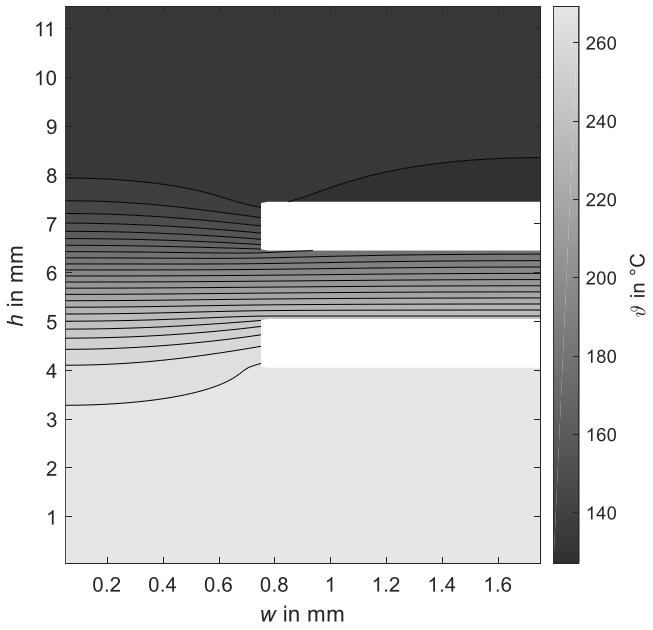

Figure 5: Temperature distribution between two half channels with adiabatic boundary conditions (not in scale)

Since the heat transfer is modelled by a simple single layer plate configuration in ATHLET, the correct thermal resistance must be specified by selecting adequate values for the plate width and thickness. As mentioned before the plate width should be the perimeter of the channel. When this parameter is fixed an effective plate thickness can be determined by comparing the thermal resistance of the simulated configuration to the simple plate configuration used in ATHLET. For the comparison the mean value of the heat transfer coefficient and the wall temperature along the channel length are calculated. Then the effective plate thickness can be determined by applying the mean values to both sides of the simple plate configuration. This calculation is conducted for various flow conditions inside the channels in order to evaluate if a constant value of δ is sufficient to describe the heat transfer characteristic of this configuration.

DOI: 10.17185/duepublico/48874

Graphically the effective plate thickness can be interpreted as a mean distance for the heat transfer between the two channels. The resulting value is always higher than the geometrical distance between the channels. Boundary effects like heat losses are not considered because they were assumed negligible.

Since the heat transfer coefficient is temperature dependent, its local value also varies along the channel perimeter in addition to the local value of the wall temperature. However, in ATHLET the heat transfer coefficient and the temperature difference are constant in one subvolume and, therefore, also along the channel perimeter. If these constant values are not equal to the mean values of the real configuration, then a correction factor C_{corr} is required in the equation of the transferred power $\dot{Q}$, given by

$$\dot{Q} = C_{corr} h A \Delta T. \quad (1)$$

Mathematically, the correction factor is the product of the correction factors of the heat transfer coefficient h and the temperature difference ΔT. The exact value of the factor depends on the set-up and on the conditions inside the channels. Its value can also be determined from the steady state heat conduction analysis. If the factor is constant, it can be included in the plate width calculation.

Heat transfer

The heat transfer coefficient h is calculated by using correlations on both sides. For the sCO_2 side, the heat transfer coefficient is calculated with the Gnielinski correlation [8], which is valid for Reynolds numbers between 2300 and 10^6 and Prantl numbers from 0.6 to 2000. Reynolds, Prandtl and Nusselt number including the friction factor ξ can be calculated by

$$Re = \frac{\rho u d_h}{\eta}, \quad (2)$$

$$Pr = \frac{\eta c_p}{\lambda}, \quad (3)$$

$$Nu = \frac{\left(\frac{\xi}{8}\right)(Re-1000)Pr}{1+12.7\sqrt{\left(\frac{\xi}{8}\right)}(Pr^{2/3}-1)}, \quad (4)$$

$$\xi = (1.82\log(Re) - 1.64)^{-2}. \quad (5)$$

For the proximity to the critical point, different modified correlations have been proposed. However, the best correlation must still be identified. Additionally, the conducted experiments are at least 2.1 MPa above the critical point. Moreover, the impact of a modified correlation on the overall heat transfer would be quite small, as it will be explained in the results section. Therefore, no further modified correlation was implemented on the sCO_2 side. On the H_2O side, two regimes occur, namely first film condensation and afterwards forced convection to the liquid. For the film condensation, the ATHLET correlations were improved and now the correlations given in [9], [10] are used. The Nusselt number is calculated for the laminar and turbulent film taking into account the film Reynolds number

$$Re_f = \frac{\dot{m}_f}{\eta_f b} = \frac{(\rho u)_f (1-\varepsilon) d_h}{4\eta_f} = 0.25 Re(1-\varepsilon), \quad (6)$$

with the liquid film mass flow rate $\dot{m}_f$, the viscosity of the film η_f and the width of the cooling surface b. In this case, b is equal to the perimeter of the channel. Applying the common relation for the hydraulic diameter $d_h = 4A_c/U_c$, the equation can be transformed to the form implemented in ATHLET. However, it is important to note that the film Reynolds number differs by a factor of 0.25 and one minus the void fraction ε from the common definition of the Reynolds number used in ATHLET [11]. The film Reynolds number increases with increasing $\dot{m}_f$ and decreasing ε. The correlation of the Nusselt number for the laminar film [9], [10], which dominates the heat transfer on the steam side, is given by

$$Nu_f = \frac{h_f \sqrt[3]{\nu_f/g}}{\lambda_f} = 0.693 \left(\frac{1-\rho_v/\rho_f}{Re_f}\right)^{1/3}. \quad (7)$$

The properties ν_f, λ_f and ρ_f are determined at the film temperature, which is the average of the wall surface and fluid bulk temperature. To reduce the calculation effort, for ρ_f the density at liquid saturation is taken in ATHLET. The vapor bulk density ρ_v is calculated at the bulk temperature and g is the acceleration due to gravity. Equation 7 contains a factor ${Re_f}^{-1/3}$, which results in a decreasing Nusselt number for increasing $\dot{m}_f$, which is reasonable because the liquid film at the wall inhibits the heat transfer. The turbulent Nusselt equation is completely empirical and more complicated. In this region, the Nusselt number increases again with increasing Re_f. The laminar and turbulent equation are combined together, including a few correction factors. However, due to the small size of the channels, the heat transfer coefficient is dominated by the laminar equation.

The basic Nusselt correlation for laminar film condensation was derived analytically for steam condensing on a vertical plane and flowing down driven by gravity. Depending on the real configuration, different shear stress corrections can be applied. Since, the H_2O flows downward driven by gravity and a small circulation pump, the model for "vertical pipe, rectified flow" [9] is most applicable. However, the ATHLET CHX simulations yield the same velocity for the gas and liquid phase. Consequently, the relative velocity and the shear stress is zero and therefore the "uncorrected" equation is used. Additionally, the small size of the channels might affect the heat transfer. Since the exact contribution of small channels is unclear, the effect is neglected in this analysis for both, sCO_2 and H_2O.

The heat conduction through the plate is modeled as described in ATHLET Models and Methods [11]. The plate is modeled as a single layer and for the material properties, the built in functions of austenitic stainless steel are used. In the input the thickness of the plate must be specified. The thickness of the plate can be chosen equal to the direct distance between the

DOI: 10.17185/duepublico/48874

channels. However, a slightly higher value might be more realistic, because heat transfer occurs over the whole surface of the channel as mentioned before. Since the heat flow is perpendicular to the isotherms, the average conduction length is longer than the direct distance. The influence of the chosen thickness is analyzed in the results section in more detail.

Pressure drop

The occurring pressure drop on the sCO_2 side can be sub-divided into the pressure drop of the inlet plenum, the channel pressure drop and the outlet plenum pressure drop. The pressure drop in the channel is derived from the Colebrook equation, which is recommended for normal pipes as well as for mini-channels [12]. The implicit correlation is approximated explicitly according to [11]. In order to calculate the channel pressure drop the wall roughness of the channel must be provided. The inlet and outlet plenum pressure drop can also be calculated with the equation used in ATHLET [11],

$$\Delta p_{plenum} = \xi_{form} \frac{\dot{m}^2}{2\rho}. \quad (8)$$

An appropriate value for the loss coefficient ξ_{form} must be given for the inlet and the outlet plenum. A single from loss is not sufficient for both plenums because the inlet and the outlet density are different depending on the amount of transferred heat. In order to determine the coefficients a single sCO_2 channel with constant heat input over the channel length was modelled in Matlab. The model solves the momentum conservation equation including the ATHLET correlations and determines the form loss coefficients by a best-fit method, minimizing the deviation between the experimental and simulated pressure drop. Instead of a constant heat input per channel length, it is also possible to implement the heat transfer and energy conservation equations to improve the best-fit method further. However, it was found that the first simple method provides good results, as shown in the results section.

RESULTS AND DISCUSSION

The correction factor for the transferred power given in Equation 1 and the effective thickness of the plate are determined by performing the two dimensional heat conduction calculations for various conditions covering the entire experimental range. For all simulated cases, the effective thickness is around 3.3 mm and the correction factor is around unity. The deviations are smaller than 6 % for both parameters. Therefore, no adaption of the plate width is necessary and it is chosen equal to the channel perimeter, which is 6 mm. The form loss coefficients for the inlet and outlet plenum, derived with Matlab, are 27.75 and 2.71, respectively. These coefficients must be divided by the square of channel cross sectional area for the use in equation 8 and in ATHLET. For the wall roughness of the channels, a value of 5 µm was selected. The influence of the number of subvolumes in the CHX was analyzed by varying the number between 5 and 40. An increasing number of subvolumes leads to a higher accuracy but also to a higher calculation effort. It was found that the calculation time increases almost linearly with the number of subvolumes. Finally, 10 subvolumes were chosen because a further increase to 40 subvolumes changes the transferred power only by less than 2 %. Decreasing the number of subvolumes to 5 subvolumes leads to a unstable transient behavior. Consequently, 10 subvolumes yield a fast and accurate representation of the CHX.

Heat transfer

Figure 6 displays the deviation of the simulated transferred power from the experimental values. Only four cases deviate by more than 10 % from the experimental value. The maximum deviation is 11.7 %. All higher deviations occur at lower transferred powers where less experimental data are available. Moreover, all but one simulated value are in the interval which is defined by the transferred power for H_2O and sCO_2, derived from the experiments. In addition, the only value, which is located outside the interval, differs by less than 1 % from the mean experimental value. This is no contradiction because for this case the power calculated from the experimental values agree very well with each other. The difference between the power calculated from the experimental values for H_2O and sCO_2 can be explained by the experimental set-up and the measurement accuracy, as described in the experimental section. Altogether the simulation predicts the experimental values very well. Therefore, no further adaptions to the heat transfer correlations were considered here, as mentioned in the last section. The slight over-prediction of the transferred power might be related to the fact that heat losses were neglected in the simulations.

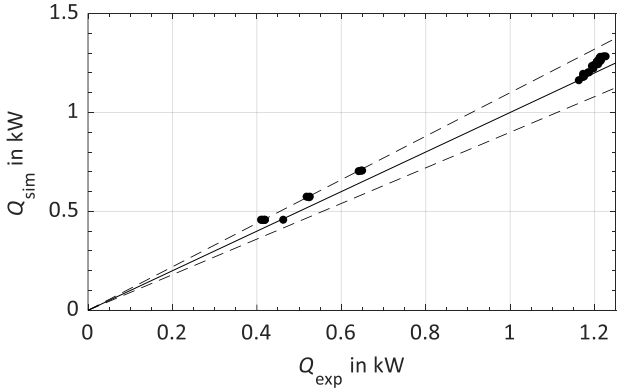

Figure 6: Simulated transferred power compared to the experimental values, in between the dashed lines the deviation is less than 10 %

In the following, case 5 of the experiments is discussed as an example. The boundary conditions for this case are given in the experimental section (Table 1). The simulated temperature profile of case 5 is shown in Figure 7. It includes the sCO_2 and H_2O bulk temperature and the wall temperature on both sides. The wall temperature, as well as the heat transfer coefficient and the transferred power are calculated per subvolume. Therefore, these values are plotted over the midpoint of each subvolume. On the left side of the diagram, the sCO_2 inlet and the H_2O outlet

DOI: 10.17185/duepublico/48874

are located. Due to the high heat capacity rate of sCO_2 compared to H_2O and the high overall heat transfer coefficient during the film condensation, the steam is condensed completely in the first third of the heat exchanger starting from the H_2O inlet. After the condensation forced convection cools down the water further. In ATHLET, the two regimes are connected with a cosine-shape interpolation. Therefore, the transition is smooth and does not cause numerical difficulties.

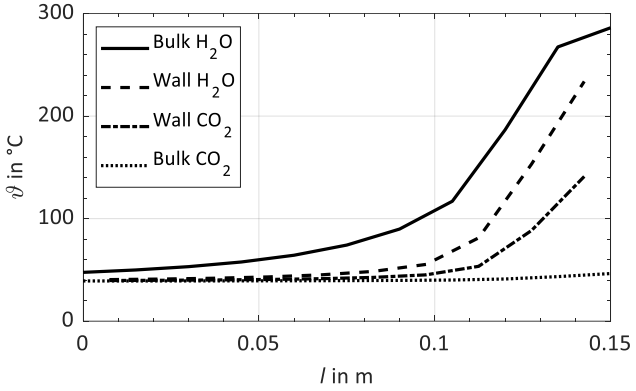

Figure 7: Simulated temperature profile in the CHX for case 5

The cosine-shape interpolation used in ATHLET is controlled by the void fraction, which is displayed in Figure 8. For a void fractions higher than zero and lower than 0.03 the two regimes are interpolated. From Figure 8 it is also visible that the steam quality drops below zero before the void fraction reaches zero. Therefore, at the end of the condensation process the steam is subcooled before it condenses completely. This effect is due to the ATHLET models which allow meta-stable states.

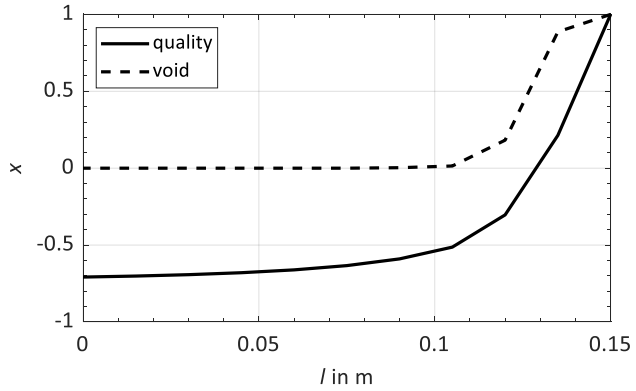

Figure 8: Steam quality and void fraction for case 5

During the film condensation the heat transfer coefficient on the H_2O side, displayed in Figure 9, is relatively high starting at 16 kW/m²K. The coefficient declines due to the increasing film thickness, which inhibits the heat transfer. The sCO_2 heat transfer coefficient is also relatively high with 4 kW/m²K at the sCO_2 outlet. However, compared to H_2O the coefficient is about two to four times lower during the condensation process. Therefore, the wall temperature is close to the H_2O temperature. After the condensation, the heat transfer coefficient of H_2O drops below 2 kW/m²K. As a result of the low H_2O side heat transfer coefficient, the wall temperature is close to the sCO_2 temperature in this section of the heat exchanger. Since the average of the wall temperature and sCO_2 bulk temperature, which is used for the calculation of the heat transfer coefficient, is close to the pseudo-critical temperature, the heat transfer coefficient of sCO_2 increases further. The peak in the heat transfer coefficient on the sCO_2 side is mainly caused by the peak of the specific heat capacity at the pseudo-critical point.

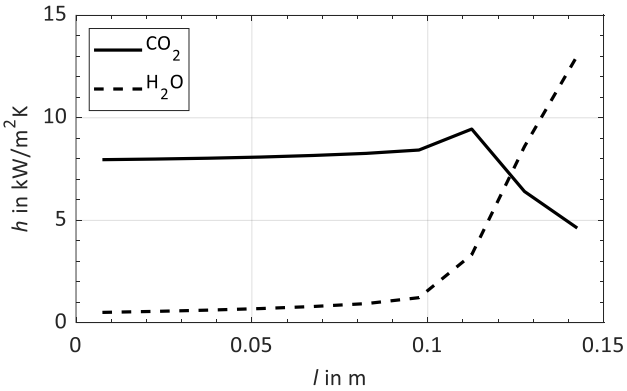

Figure 9: Simulated heat transfer coefficients for H_2O and sCO_2 for case 5

Close to the critical pressure and pseudo-critical temperature, improved correlations might provide the sCO_2 heat transfer coefficient with a higher accuracy. However, due to the low H_2O side heat transfer coefficient, the overall heat transfer coefficient and, therefore, the simulation results are affected scarcely. Thus, in this case no adaption of the heat transfer correlation is necessary. Summarizing, during the condensation, the sCO_2 side limits the overall heat transfer coefficient. After the condensation, the low heat transfer coefficient on the H_2O side strongly inhibits the heat transfer.

Because of these two facts, almost all the heat is transferred in the section where the condensation takes place. This is directly visible from the transferred power per channel length, shown in Figure 10. To maximize the transferred power, it is desirable to extend the condensation section. This can be achieved by a higher H_2O or a lower sCO_2 mass flow rate. In the current experimental set-up, the H_2O mass flow rate is restricted by the maximum electrical heating power of the evaporator with 1.6 kW. Moreover, the sCO_2 test facility introduces a lower bound on the sCO_2 mass flow rate. Furthermore, two additional effects prevent a higher total transferred power. Firstly, the Reynolds number is decreasing with decreasing sCO_2 mass flow rate and, therefore, the heat transfer coefficient on the sCO_2 side is also decreasing. Secondly, a lower sCO_2 mass flow rate leads to higher sCO_2 bulk temperatures. As a result, the average temperature, which is relevant for the determination of the heat transfer coefficient, also increases and departs from the pseudocritical temperature. This mainly decreases the specific heat capacity, which directly results in a decrease of the heat transfer coefficient.

DOI: 10.17185/duepublico/48874

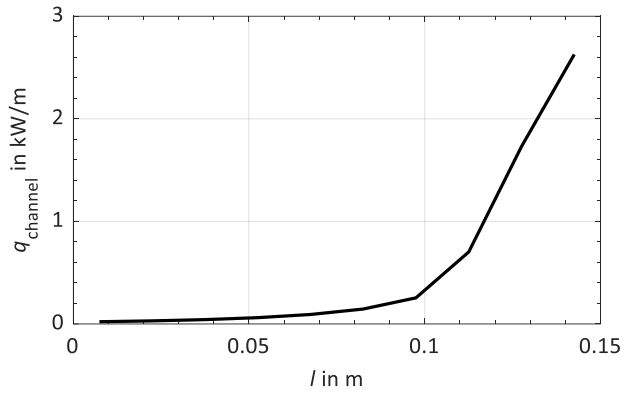

Figure 10: Simulated transferred power per channel length for case 5

Pressure drop

In Figure 11, the simulated and measured pressure drops on the sCO_2 side are compared. All but one case yield a deviation of less than 10 %. Therefore, it seems appropriate to model the pressure drop divided into channel, inlet and outlet pressure drop using the determined form loss coefficients, as described in the modelling section. The case with the lowest sCO_2 mass flow rate at a pressure of 11 MPa deviates by 17.4 %. For this case, the measurement might be erroneous because at low mass flow rates the control strategy of the SCARLETT test facility has lead to mass flow rate oscillations.

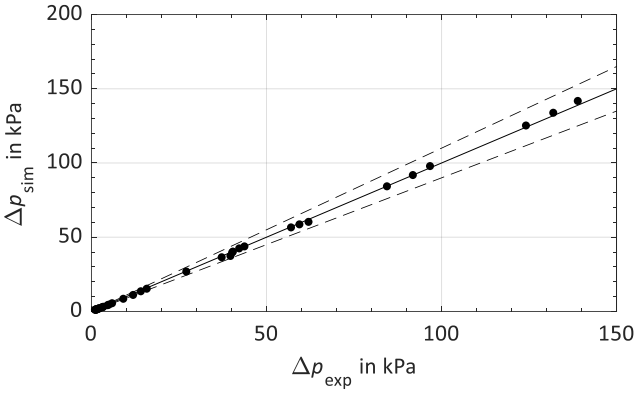

Figure 11: Simulated sCO_2 side pressure drop compared to the experimental values, in between the dashed lines the deviation is less than 10 %

In Figure 12 the sCO_2 side pressure drop of case 5 is shown. The total pressure drop of 42 kPa can be sub-divided into the inlet plenum, channel and outlet plenum pressure drop, 34 kPa, 5 kPa and 3 kPa, respectively. Probably, the perpendicular attached inlet and outlet pipes cause the high plenum pressure drops. Although, the main pressure drop can be attributed to the inlet plenum, it proved inadequate to model the pressure drop with just one form loss coefficient for the inlet plenum, because a higher sCO_2 outlet temperature yields a lower outlet density. This affects the plenum pressure drop defined in Equation 8. As mentioned before, higher outlet temperatures occur for cases with a low sCO_2 and high H_2O mass flow rate.

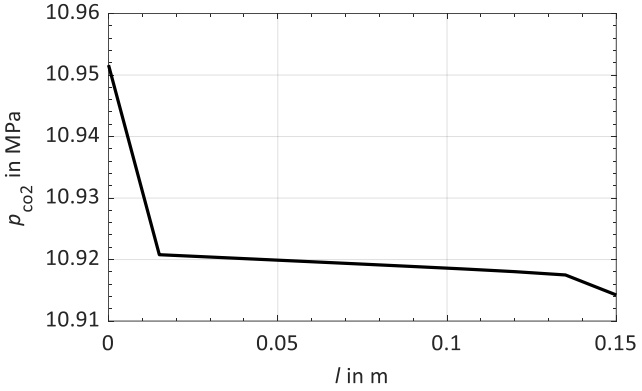

Figure 12: Simulated pressure profile for case 5

Mass flow rate variation

In order to show the influence of the H_2O and sCO_2 mass flow rates on the transferred power, a variation covering the experimental mass flow range was conducted. The results are provided in Figure 13. Over the whole range, the influence of the sCO_2 mass flow rate on the transferred power is almost negligible. Since the overall heat transfer coefficient during the condensation is high, the condensation of the steam takes up less than half of the heat exchanger length, for many cases even less than a quarter. The remaining length is more than sufficient to cool down the condensed steam independent of the sCO_2 mass flow rate. Only for very low sCO_2 and high H_2O mass flow rates the influence of the low Reynolds number on the sCO_2 side, which inhibits the heat transfer during the condensation and in the cool down phase, becomes visible. On the contrary, for high sCO_2 and H_2O mass flow rates, the investigated heat exchanger could transfer considerably more power and would still be able to condense and cool down the steam.

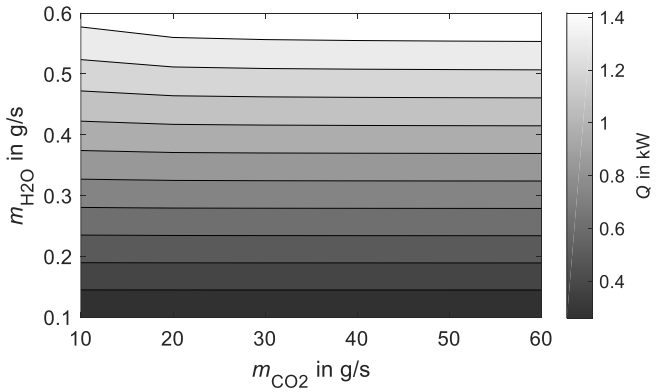

Figure 13: Influence of H_2O and sCO_2 mass flow rate on the transferred power for a sCO_2 inlet pressure of 11 MPa

CONCLUSION

In this study, a correlation based modelling approach for a sCO_2 compact heat exchanger (CHX) is investigated. Since no special CHX model exists in ATHLET, the general modelling

DOI: 10.17185/duepublico/48874

approach for co-current and counter-current flow arrangements is applied. Instead of modelling the whole heat exchanger, only one representative channel pair is modelled and the results are scaled with the number of channel pairs. The channels are divided in subvolumes and the local heat transfer coefficient and pressure drop are calculated with correlations. For sCO_2 the Gnielinski and the Coolebrook correlation are used.

In order to prove the validity of the modelling approach for the sCO_2/H_2O CHX, a model of a two-plate CHX is prepared in ATHLET and the simulation results are compared with experimental results. The form loss coefficients, which describe the inlet and outlet plenum pressure drop, are calculated with a best-fit method using a simple model for one sCO_2 channel. Additionally, the effective plate thickness is determined by a two dimensional steady state heat conduction calculation. For CHX with more plates and channels, e.g. for nuclear power plant applications, the effective plate thickness is considerably lower compared to the two-plate configuration.

In general, the results of the ATHLET simulations are in good agreement with the experimental values. Compared to the mean value of the experiments, almost all simulated cases yield a deviation of less than 10 % concerning the transferred power and the pressure drop on the sCO_2 side.

A closer evaluation reveals that most of the heat is transferred in the section of the heat exchanger, where steam condensation takes place. Since the heat transfer coefficient on the H_2O side is high during the condensation, the sCO_2 side, still being quite high, limits the overall heat transfer coefficient. After the condensation, the relation is inverted because the heat transfer coefficient of liquid H_2O is significantly lower for the investigated set-up. Considering the effective plate thickness, the influence of thermal resistance of the wall is almost negligible except for the small impact during the condensation phase. Moreover, an improved heat transfer correlation for sCO_2 for states close to the pseudocritical temperature would scarcely change the results because only downstream the condensation section, when the H_2O heat transfer coefficient is inhibiting the overall heat transfer phase, the temperature relevant for the determination of the heat transfer coefficient is close to the pseudocritical temperature. Future investigations will analyze this relation further. Finally, a variation of the H_2O and sCO_2 mass flow rate confirmed the minor impact of the sCO_2 mass flow rate. Furthermore, since less than half of the heat exchanger length is necessary for the condensation of the steam, the investigated CHX could transfer considerably more power or be shortened by 50%

In the future, more experiments will be analyzed to further validate the proposed approach. Moreover, cooling and cross-flow will be considered where either improved correlations or new models are necessary. After the model development and validation, the complete sCO2-HeRo system, attached to a boiling or pressurized water reactor, will be simulated in ATHLET.

NOMENCLATURE

A	heat transfer area of heat exchanger (m²)
A_c	channel cross sectional area / flow area (m²)
b	width of the cooling surface (m)
C_{corr}	correction factor (-)
c_p	specific isobaric heat capacity (J/kgK)
d_h	hydraulic diameter (m)
h	heat transfer coefficient (W/m²K)
l	length of heat exchanger (m)
$\dot{m}$	mass flow rate (kg/s)
Nu	Nusselt number (-)
p	pressure (MPa)
Pr	Prandtl number (-)
$\dot{Q}$	transferred power (W)
$\dot{q}$	transferred power per length (W/m)
Re	Reynolds number (-)
T	temperature (K)
u	velocity (m/s)
U_c	perimeter of one channel (m)
w	width of the plate (m)

Greek letters

δ	effective plate thickness (m)
Δl	length of one subvolume (m)
ε	void fraction (-)
η	dynamic viscosity (Pa/s)
ϑ	temperature (°C)
λ	thermal conductivity (W/mK)
ν	kinematic viscosity (m²/s)
ξ_{form}	form loss coefficient of plenum (m^{-4})
ρ	density (kg/m³)

Subscripts

exp	experiment
f	film
s	simulation

Acronyms

BWR	boiling water reactor
CHX	compact heat exchanger
H_2O	water/steam
HeRo	heat removal system
sCO_2	supercritical carbon dioxide

ACKNOWLEDGEMENTS

The presented work was funded by the German Ministry for Economic Affairs and Energy (BMWi. Project no. 1501557) on basis of a decision by the German Bundestag.

 DOI: 10.17185/duepublico/48874

REFERENCES

[1] J. Venker, "Development and Validation of Models for Simulation of Supercritical Carbon Dioxide Brayton Cycles and Application to Self-Propelling Heat Removal Systems in Boiling Water Reactors," University of Stuttgart, IKE 2 – 156, 2015.

[2] "sCO2-HeRo." [Online]. Available: http://www.sco2-hero.eu/. [Accessed: 19-Feb-2019].

[3] D. Bestion, "System code models and capabilities," in *THICKET*, 2008, pp. 81–106.

[4] G. Mauger, N. Tauveron, F. Bentivoglio, and A. Ruby, "On the dynamic modeling of Brayton cycle power conversion systems with the CATHARE-3 code," *Energy*, vol. 168, pp. 1002–1016, 2019.

[5] L. Batet *et al.*, "Modelling of a supercritical CO2 power cycle for nuclear fusion reactors using RELAP5–3D," *Fusion Eng. Des.*, vol. 89, no. 4, pp. 354–359, Apr. 2014.

[6] M. J. Hexemer, H. T. Hoang, K. D. Rahner, B. W. Siebert, and G. D. Wahl, "Integrated Systems Test (IST) Brayton Loop Transient Model Description and Initial Results," in *S-CO2 Power Cycle Symposium*, 2009, pp. 1–172.

[7] M. R. Straetz, R. Mertz, and J. Starflinger, "Experimental investigation on the heat transfer between condensing steam and sCO2 in a compact heat exchanger," *2nd Eur. sCO2 Conf. 2018*, Aug. 2018.

[8] G. F. Hewitt, *Heat exchanger design handbook*. New York: Begell House, 1998.

[9] P. von Böckh and T. Wetzel, *Wärmeübertragung: Grundlagen und Praxis*, 7th ed. Berlin: Springer, 2017.

[10] R. Numrich and J. Müller, "J1 Filmkondensation reiner Dämpfe," in *VDI-Wärmeatlas*, Berlin, Heidelberg: Springer Berlin Heidelberg, 2013, pp. 1011–1028.

[11] H. Austregesilo *et al.*, "ATHLET Models and Methods," Garching, 2016.

[12] V. Dostal, M. J. Driscoll, and P. Hejzlar, "A Supercritical Carbon Dioxide Cycle for Next Generation Nuclear Reactors," *Tech. Rep. MIT-ANP-TR-100*, pp. 1–317, 2004.

DOI: 10.17185/duepublico/48874

DOI: 10.17185/duepublico/48874
URN: urn:nbn:de:hbz:464-20190927-134543-4